

# The determination of the constant phase of seismic wavelet using automatic seismic-well tying

Hao Wu, Bo Zhang & Danping Cao

To cite this article: Hao Wu, Bo Zhang & Danping Cao (2019) The determination of the constant phase of seismic wavelet using automatic seismic-well tying, *Exploration Geophysics*, 50:3, 245-254, DOI: [10.1080/08123985.2019.1595577](https://doi.org/10.1080/08123985.2019.1595577)

To link to this article: <https://doi.org/10.1080/08123985.2019.1595577>



Published online: 07 May 2019.



Submit your article to this journal [↗](#)



Article views: 14



View Crossmark data [↗](#)



## The determination of the constant phase of seismic wavelet using automatic seismic-well tying

Hao Wu<sup>a</sup>, Bo Zhang<sup>a</sup> and Danping Cao<sup>b</sup>

<sup>a</sup>Department of Geological Science, The University of Alabama, Tuscaloosa, United State; <sup>b</sup>School of Geoscience, China University of Petroleum (East China), Qingdao, China

### ABSTRACT

Seismic wavelet estimation is the bedrock of seismic-well tying and seismic inversion but remains a challenge. Huge amounts of effort have been expended on seismic wavelet estimation and determining the amplitude and phase spectrum is a time-consuming task. In this article, we develop a workflow to determine automatically the constant phase of an estimated wavelet. This workflow begins with statistical wavelet estimation and seismic-well tying. We then extract a new seismic wavelet with a constant phase by using the well and seismic data together. To obtain the best phase for the extracted wavelet using well and seismic data, we rotate the phase of the wavelet by a user-defined increment and perform automatic seismic-well tying for each phase-rotated wavelet. The phase that reaches the maximum correlation coefficient between the synthetic and seismic data is regarded as the best phase for wavelets in each iteration. We next update the time–depth relation using the best seismic-well tie (the maximum correlation coefficient). We repeat the wavelet estimation using well and seismic data, phase rotation, automatic seismic-well tying and time–depth updating until the difference between wavelets, and time–depth relationships, in the current and previous iterations is below a user-defined threshold.

### ARTICLE HISTORY

Received 1 December 2017  
Accepted 2 September 2018

### KEYWORDS

Seismic-well tie; wavelet; phase; DTW

### Introduction


Seismic wavelet estimation is a key procedure in seismic interpretation and inversion. Determination of a seismic wavelet includes estimates of the amplitude and phase spectrum. Wavelet estimation methods can be classified into three main categories: (1) direct deterministic measuring of the wavelet, (2) statistical extraction of the wavelet from the seismic data and (3) extraction of the wavelet using well log and seismic data. Deterministic methods require that a seismic-well tie already exists, whereas the statistical method extracts an average wavelet from a specified window of 3D seismic data (Edgar and van der Baan 2011). Wavelet estimation using well and seismic data incorporates the “prior” reflectivity information in the wavelet estimation (Richard and Brac 1988). Statistical wavelets can be estimated from the seismic data only without appealing to well logs. Most statistical wavelet estimations are based on an assumption that seismic traces are a convolution of the earth’s reflectivity and a temporally and spatially invariant zero or minimum phase wavelet. Statistical wavelets assume that the autocorrelations of amplitude spectra of the seismic data are approximately equal to the seismic wavelet (Yilmaz 2001).

Determining the phase spectrum of a seismic wavelet is as important as determining the amplitude

spectrum. Van der Baan (2008) showed that a phase mismatch might result in incorrect horizon picking or seismic-well tying. Many techniques have been developed to identify the phase seismic wavelet phase spectrum. Compared with an amplitude spectrum estimation of seismic wavelets, determining the phase spectrum is far more difficult and affects seismic inversions significantly (Hampson 2007). Wiggins (1978) estimated the phase of seismic wavelets using minimum entropy deconvolution. This technique does not require assumption of the phase characteristics of a seismic wavelet. White (1988) proposed estimating the phase of a seismic wavelet by integrating maximum kurtosis theory. The advantage of White’s method is that there is no requirement for a Gaussian distribution of the subsurface reflectivity series. Levy and Oldenburg (1987) present a method that uses the varimax norm to estimate the residual phase directly; this method can perform phase corrections automatically. Van der Baan (2008) developed a method based on maximum kurtosis estimation to obtain time-varying wavelets and this is robust enough to detect time-varying phase changes.

Hampson (2007) pointed out that constant phase wavelet estimation using well data is the most robust method. Estimation of the amplitude and phase spectrum of a wavelet using seismic data does not consider

**CONTACT** Bo Zhang  [bzhang33@ua.edu](mailto:bzhang33@ua.edu)  Department of Geological Science, The University of Alabama, 2003 Beville Building, +1 (205)348-5095

 Supplemental data for this article can be accessed here. <https://doi.org/10.1080/08123985.2019.1595577>

“prior” reflectivity information contained in the well logs (Richard and Brac 1988). There are two main steps in wavelet estimation using seismic and well data. The first includes amplitude spectrum estimation using seismic data and reflectivity computed using well logs. The second is to obtain the optimum phase of the wavelet through seismic–well tying. Nyman, Parry, and Knight (1987) proposed an interactive methodology for estimation of a seismic wavelet using well control. Their method estimated the wavelet amplitude and phase spectrum separately. The amplitude estimation involves simply averaging the ratio between the seismic traces and the reflectivity spectrum. Nyman, Parry, and Knight (1987) assumed a constant phase spectrum and obtained it using phase and time shifting, which maximized correlation with the synthetic and seismic traces. To obtain the optimal wavelet phase and time shift for the seismic–well tie, usually requires more than ten manual seismic–well ties and phase scanning of the seismic wavelet, which is therefore time-consuming. Richard and Brac (1988) estimated a linear phase wavelet using well-control. Buland and Omre (2003) proposed to estimate the wavelet from seismic and well data using a Bayesian theory. In this paper, we propose a workflow to expedite estimation of the constant phase of a seismic wavelet in seismic–well tying. Our workflow is similar to that proposed by Hampson (2007). However, our method can expedite phase determination. We replace manual optimum phase determination with an automatic procedure. We first scan the phase rotation of the wavelet according to the user-defined range and increment step. We then automatically obtain the corresponding time shift, synthetic squeezing and stretching for each candidate phase using dynamic time warping (DTW) (Sakoe and Chiba 1978). The phase that yields the largest correlation coefficient between the seismic and synthetic traces is considered the best phase in the current loop of the seismic–well tie. We then estimate the amplitude of a wavelet using the new time–depth relationship. We next scan the phase and automatically perform seismic–well ties for each phase-rotated wavelet. We repeat the procedure of amplitude estimation using well-log data, phase scanning and automatic seismic–well ties until we converge on a solution.

## Methodology

A stacked seismic trace can be regarded as a convolution of the seismic wavelet with reflectivity series and added noise:

$$x = r * w + n \quad (1)$$

where  $x$  is the seismic trace,  $r$  is the reflectivity series,  $w$  is the wavelet,  $n$  is the noise, and  $*$  denotes the convolution operator. A wavelet is usually considered a transient signal. It has a start time and an end time, and its

energy is confined between these two positions (Yilmaz 2001).

Seismic–well tying is the procedure of matching the synthetic seismogram computed using well logs and the wavelet to a real seismic trace near the borehole (Walden and White 1984). We compute the reflectivity series from a velocity log,  $v(z)$ , and a density log,  $\rho(z)$ . The synthetic seismogram is generated by convolving the reflectivity series with a user-defined wavelet or a wavelet estimated from the (White and Simm, 2003). Here, we use DTW to perform the seismic–well tie by automatically time shifting, stretching and squeezing the synthetic seismogram. DTW is an algorithm for measuring the similarity between two signals (Müller 2007). The objective of this algorithm is to align the two signals by time shifting, squeezing and stretching one of them.

Several researchers (Muñoz and Hale 2012; Herrera et al. 2012) have proposed use of DTW for automatic seismic–well ties. Herrera et al. (2014) adds a global distance constraint to DTW to prevent nonphysical alignment. Muñoz and Hale (2015) applied DTW for multiple well-ties. Wu and Caumon (2017) employed DTW to perform multiple seismic well ties on flattened synthetic and seismic traces. Error function computation is the first step in DTW to align two signals. We first apply ten times finer sampling for synthetic and real seismic traces. The finer interpolation of synthetic and real seismic traces realises the similar smaller time shift strain of synthetics proposed by Hale (2013). We then use the Euclidean distance between the synthetic  $\mathbf{X} = (x_1, x_2, \dots, x_N)$  and real seismic traces  $\mathbf{Y} = (y_1, y_2, \dots, y_M)$  to compute the error matrix  $d(i, j)$

$$d(i, j) = \sqrt{(x_i - y_j)^2}, \quad (2)$$

where  $i, j$  is the sample index of the refined seismic and synthetic trace, respectively. The total numbers of samples for the seismic and synthetic traces are  $M$  and  $N$ , respectively. We then compute the accumulated error matrix  $D(i, j)$  stepwise using the error matrix.

$$D(i, j) = d(i, j) + \min\{D(i-1, j-1), D(i-1, j) + d(i-2, j-1), D(i, j-1) + d(i-1, j-2)\}. \quad (3)$$

The final step of DTW is backtracking the minimum cost path within the accumulated error matrix

$$p_L = \arg \min\{D(M, 1) \dots D(M, N)\} \quad (4a)$$

$$p_{L-1} = \arg \min\{D(i-1, j-1), D(i-1, j) + d(i-2, j-1), D(i, j-1) + d(i-1, j-2)\}, \quad (4b)$$

where  $L$  is the total sample number of the backtracked path. We apply the algorithm of dynamic programming to backtrack the path of minimum accumulated

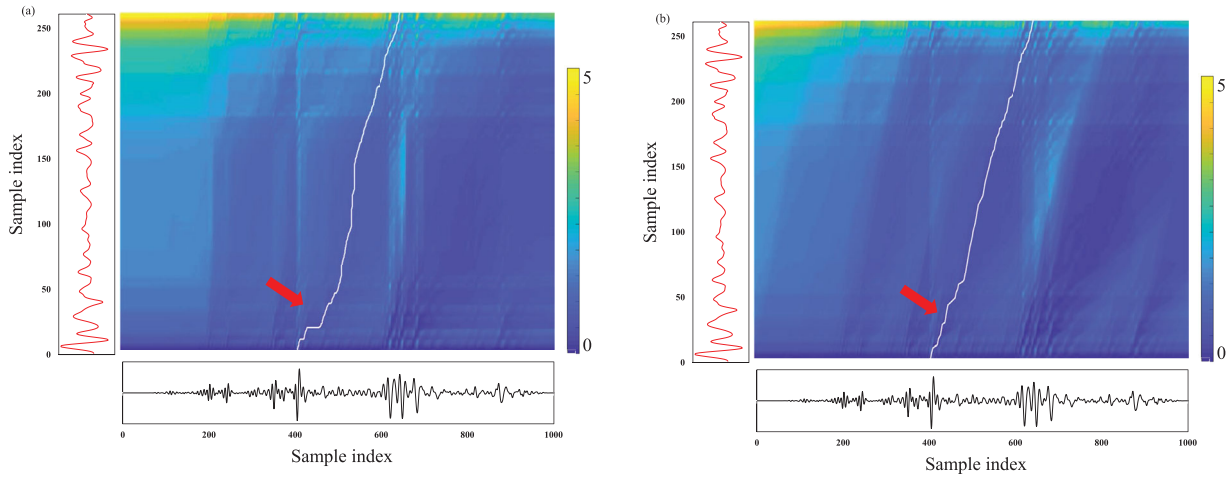


**Figure 1.** Illustration of seismic well result using original and improved dynamic time warping (DTW) algorithms. (a) Accumulated error matrix and optimal warping path using original DTW. (b) Accumulated error matrix and optimal warping path using improved DTW.

Euclidean distance to obtain a sequence of corresponding index pairs  $p = (i, j)$ , which is the best match between the synthetic and real seismic traces.

Finally, we can shift, stretch and squeeze the synthetic trace to tie it to the real seismic trace according to the tracked minimum cost path. Unfortunately, non-physical alignment is unavoidable. In other words, DTW does not consider the amount of shifting, stretching and squeezing for a near-by signal when aligned with another signal. Figure 1(a) illustrates an example of a seismic (black curve) well (red curve) tie using DTW. The red arrows indicate the locations where severe stretching of the synthetic trace is needed to tie the seismic trace. The black arrow indicates where severe squeezing of the synthetic trace is needed to tie the seismic trace. Several methods have been proposed to address this problem. Roberto et al. (2012) add a global constraint to the DTW to limit the maximum amount of permitted stretching and squeezing. Hale (2013) refine the error matrix to apply a smaller shift strain and achieve a smoother path slope. To avoid severe stretching and squeezing in the real world of a seismic-well tie, we add a weight term to the accumulated error matrix

$$\begin{aligned}
 w_{I1} &= \lambda \frac{(t_{I+1} - t_I) - (t_I - t_{I-1})}{(\tau_{I+1} - \tau_I) - (\tau_I - \tau_{I-1})} = \lambda \frac{1 - (t_I - t_{I-1})}{1 - (\tau_I - \tau_{I-1})} \\
 w_{I2} &= \lambda \frac{(t_{I+1} - t_I) - (t_I - t_{I-1})}{(\tau_{I+1} - \tau_I) - (\tau_I - \tau_{I-1})} = \lambda \frac{1 - (t_I - t_{I-1})}{2 - (\tau_I - \tau_{I-1})} \\
 w_{I3} &= \lambda \frac{(t_{I+1} - t_I) - (t_I - t_{I-1})}{(\tau_{I+1} - \tau_I) - (\tau_I - \tau_{I-1})} = \lambda \frac{2 - (t_I - t_{I-1})}{1 - (\tau_I - \tau_{I-1})}
 \end{aligned} \quad (5a)$$

$$\begin{aligned}
 p_i &= \operatorname{argmin}[D(i - 1, j - 1) + w_{I1}D(i - 1, j) \\
 &\quad + D(i - 2, j - 1) + w_{I2}D(i, j - 1) \\
 &\quad + D(i - 1, j - 2) + w_{I3}]
 \end{aligned} \quad (5b)$$

where the  $\lambda$  is the user-defined weight and  $(t_I, \tau_I)$  denotes the position index of the optimal matching path. Our proposed weight terms are the second derivative of the unwrapped path. We expect to avoid an abrupt change in unwrapped path by minimizing our weighted term. An abrupt change in the path corresponds to severe stretching or squeezing of the synthetic trace in the seismic-well tie, which can limit variation in the path slope between the last and current steps. The white curve in Figure 1(b) shows the tracked optimum cost path using Equation (5). We successfully avoid the severe stretching and squeezing shown in Figure 1(a). Figure 2(a) and 2(b) show the seismic-well tie using the unweighted and weighted backtracking methods, respectively. The cross-correlation coefficients in Figure 2(a) and 2(b) are 0.652 and 0.801, respectively.

Figure 3 shows the proposed workflow used to determine the phase of the wavelet using the improved DTW. We obtain the amplitude spectrum of proper wavelet using and seismic data and the constant phase by comparing the automatic seismic-well tie for each candidate phase. The workflow is an iterative procedure. It begins with an automatic seismic-well tie by DTW. The reflectivity is computed from the well log, and the initial wavelet is the statistical wavelet that is computed from the whole seismic trace. The next step is to extract the wavelet using well and seismic data (Hampson 2007). We then rotate the phase of the input wavelet and convolve with the reflectivity to compute a set of synthetic seismograms. We next apply DTW to make an alignment between the seismic trace and synthetic seismograms and calculate the correlation between the synthetic and seismic traces. We choose the phase that has the maximum correlation coefficients as the best phase and update the time–depth relationship of the well log. We repeat the steps of extracting the wavelet using well

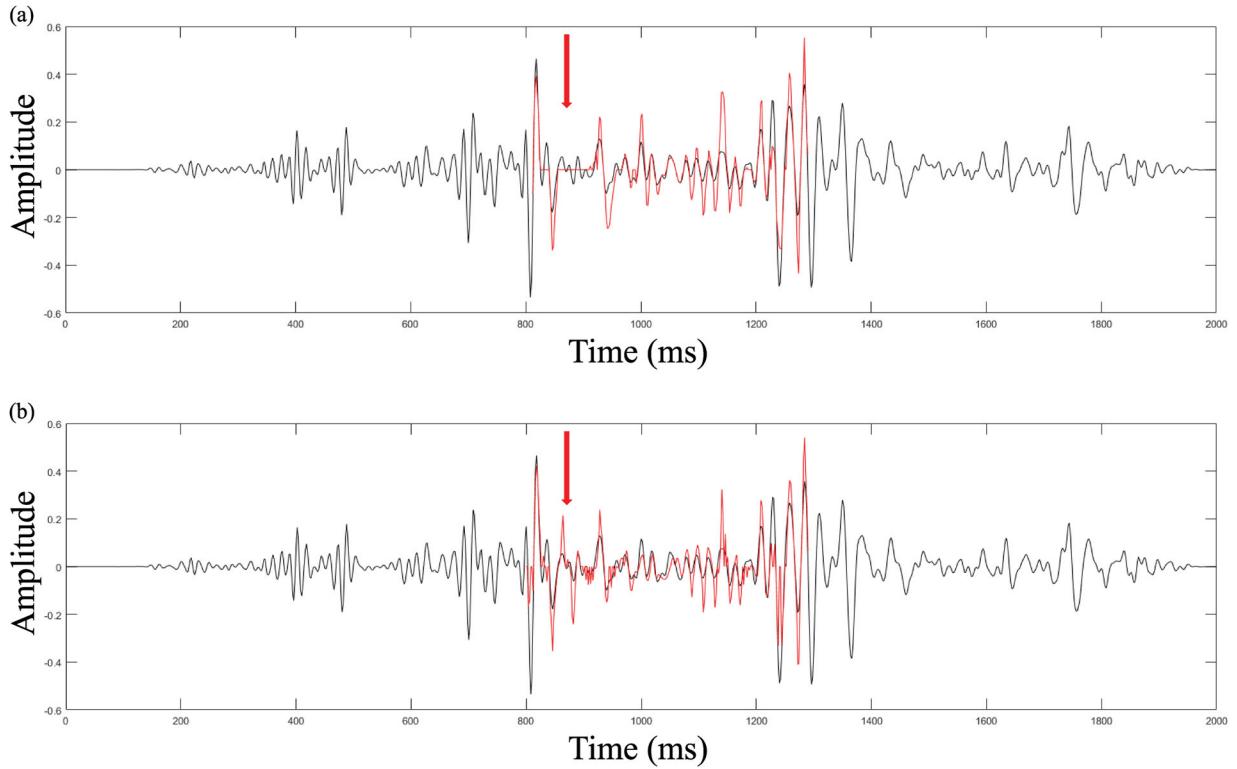


**Figure 2.** Seismic-well tie results using (a) dynamic time warping (DTW) and (b) improved DTW. The improved DTW successfully avoids severe stretching and squeezing.

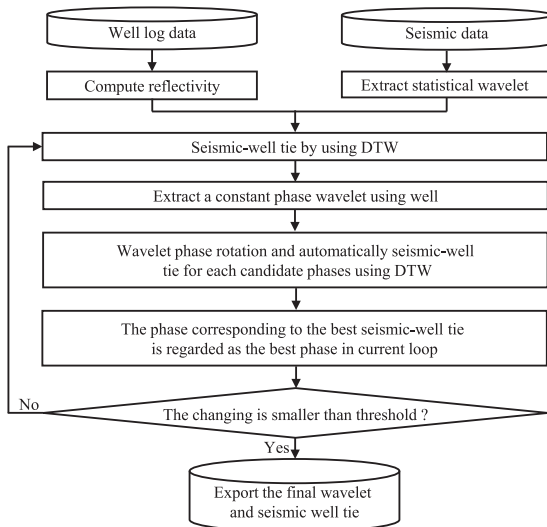


**Figure 3.** Proposed workflow for seismic phase determination.

and seismic data, phase rotation and seismic-well tying, phase selecting and time–depth relationship updating until and the wavelets and time–depth relationships in the current and previous iterations are smaller than a user-defined threshold (Equation 6).

$$\frac{\sum_i W^{(k+1)}(f_i) - W^{(k)}(f_i)}{\sum_i W^{(k)}(f_i)} < 0.001 \quad (6a)$$

$$|\phi^{(k+1)} - \phi^{(k)}| < 2 \quad (6b)$$

$$\frac{\sum |T^{(k+1)}(j) - T^{(k)}(j)|}{N} < 0.001 \quad (6c)$$

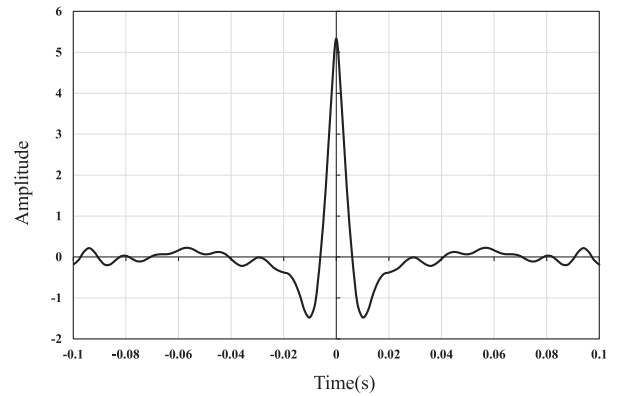


**Figure 4.** Initial statistical wavelet extracted using commercial software.

where  $W^{(k)}(f_i)$  is the amplitude spectrum of the wavelet in the  $k^{\text{th}}$  iteration of the seismic-well tie,  $\phi$  is the constant phase of the wavelet,  $T_k(i)$  is the time shift for the  $j^{\text{th}}$  sample of the synthetic trace, and  $N$  is the total sample number of the synthetic trace.

## Application

### Real data example

To demonstrate the effectiveness of our workflow, we apply it to a seismic survey acquired over the Fort Worth Basin. We use one well within the seismic survey to demonstrate the proposed workflow. Figure 4 shows the extracted 200 ms statistical wavelet from the

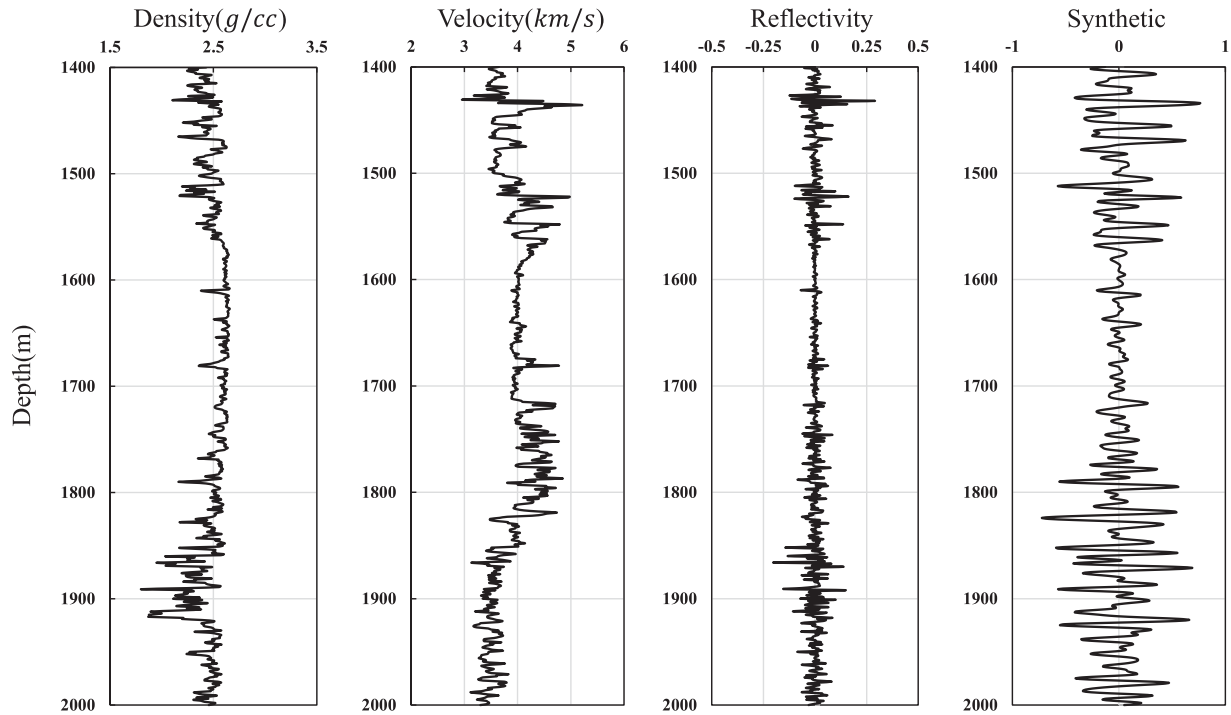


**Figure 5.** Well logs and synthetic trace used for the seismic-well tie. The first, second, third and fourth panels are the density log, velocity log, computed reflectivity and computed synthetic seismogram, respectively.

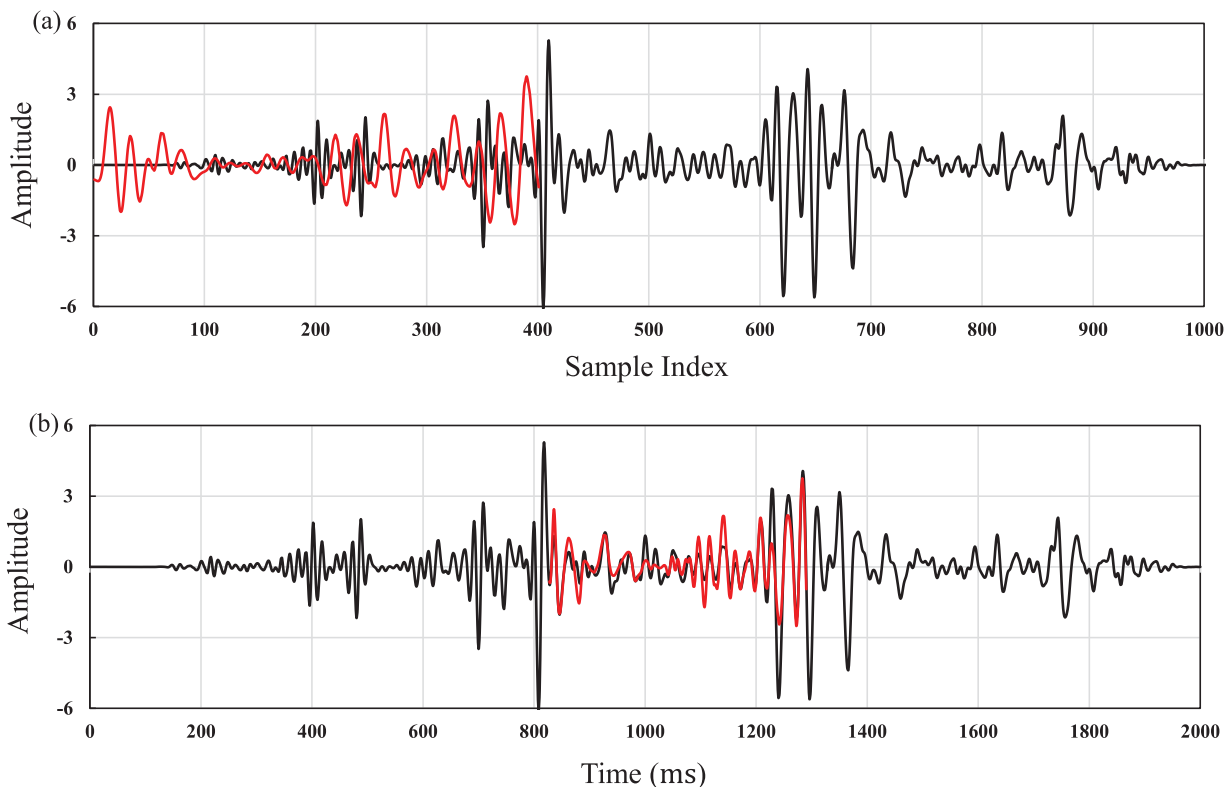


**Figure 6.** Synthetic (red) and seismic (black) traces (a) before and (b) after the seismic-well tie.

post-stack seismic using HampsonRussell commercial software. The extracted statistical wavelet is used as the initial wavelet for the seismic-well tie using DTW. The first, second, third and fourth panels in Figure 5 are the density, P-wave velocity, computed reflectivity and computed synthetic, respectively. We compute the

synthetic trace via convolution between the reflectivity shown in the third panel of Figure 5 and the wavelet shown in Figure 4. Figure 6(a) shows the synthetic trace (red curve) overlaid on the real seismic trace at the wellbore location before the automatic seismic-well tie. The horizontal axis is the sample index of the two



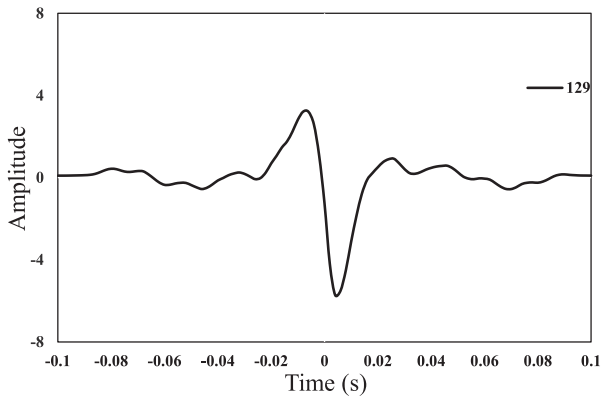


**Figure 7.** Extracted wavelet using well and seismic data in the first iteration.

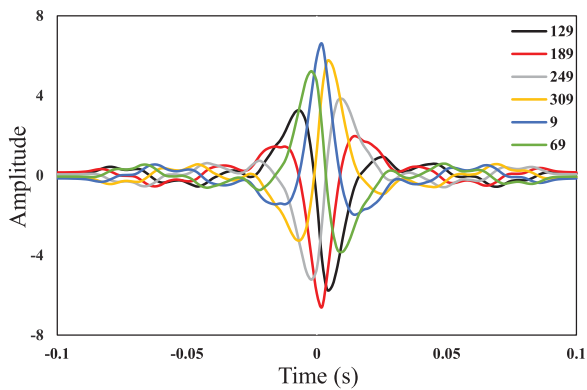


**Figure 8.** Six representative phase-rotated wavelets in the first iteration of the seismic-well tie. The initial phase of the wavelet is 129°. The phases of the phase-rotated wavelets are 129°, 189°, 249°, 309°, 9° and 69°.

sequences (synthetic and real seismic traces). In our case, we have only P-wave and density logs within a limited depth zone. The synthetic trace is much shorter

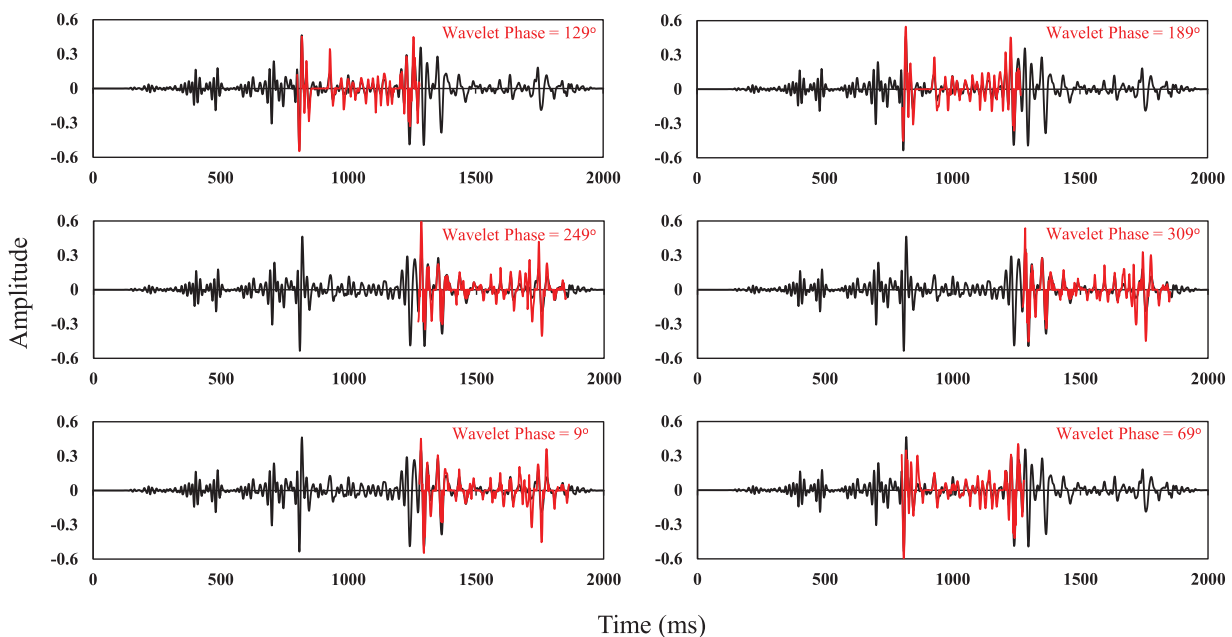


**Figure 9.** Six representative results of an automatic seismic-well tie in the first iteration for 0°, 60°, 120°, 180°, 0°, and 300° phase-rotated wavelets.

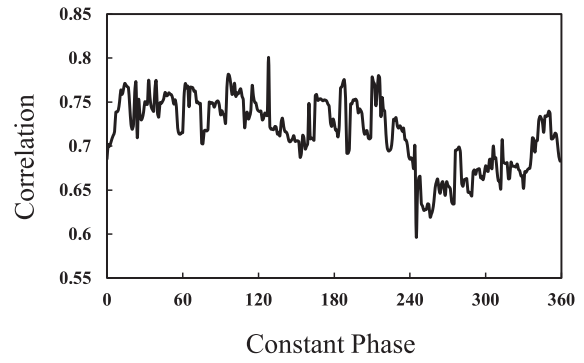


**Figure 10.** Cross-correlation coefficient between seismic-well tie for phase-rotated wavelets the first iteration.

than the seismic traces. Figure 6(b) shows the results of the automatic seismic-well tie using the statistical wavelet.

We begin our phase determination after obtaining an approximate seismic-well tie, as shown in Figure 6(b). We iteratively extract the wavelet using well and seismic data with a constant phase. Figure 7 shows the extracted wavelet using well and seismic data in the first iteration. The initial phase of the exacted wavelet shown in Figure 7 is 129°. We then rotate the phase of the wavelet and convolve the phase-rotated wavelet with the reflectivity to generate the synthetic seismogram. In this study, we rotated the phase from 0° to 359° in steps of 1°. Figure 8 shows six representative phase-rotated wavelets with rotations of 0°, 60°, 120°, 180°, 240° and 300°. The phases of the rotated wavelets shown in Figure 8 are 129°, 189°, 249°, 309°, 9° and 69°, respectively. We next apply DTW to perform the automatic seismic-well tie between the synthetic and seismic traces and compute the correlation coefficient

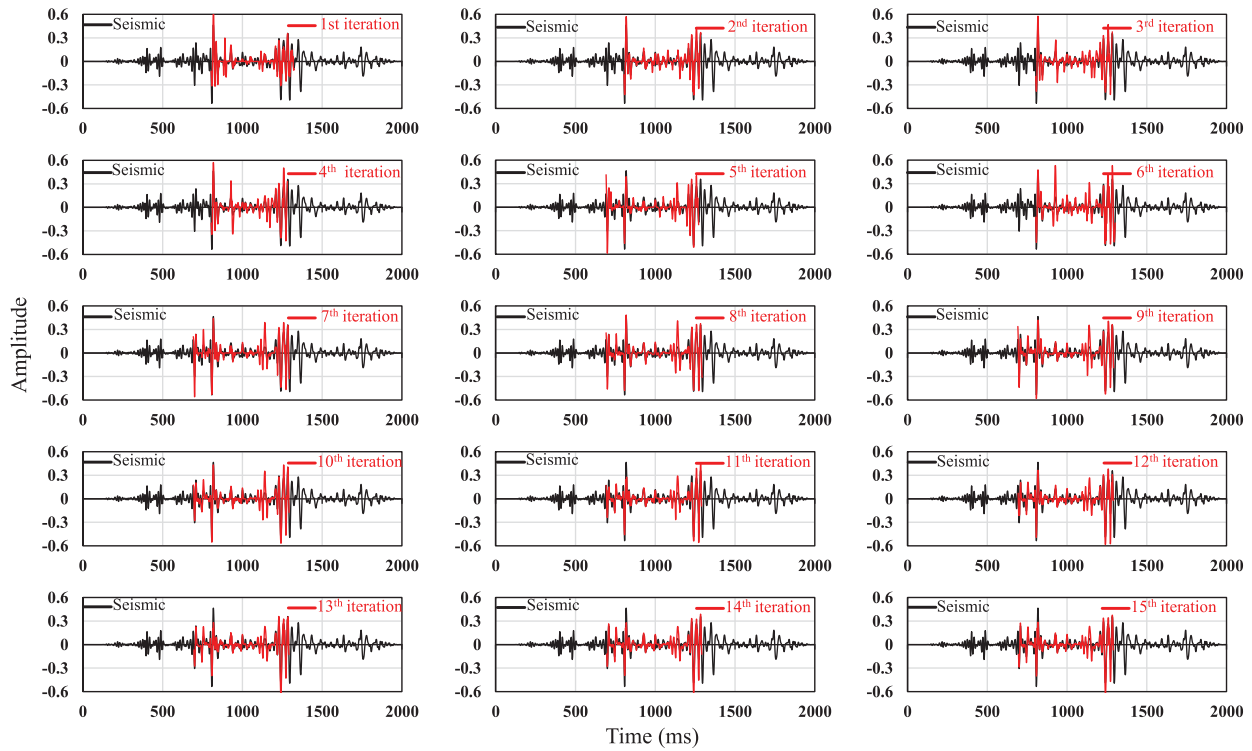


Figure 11. Seismic-well tie results in each iteration.

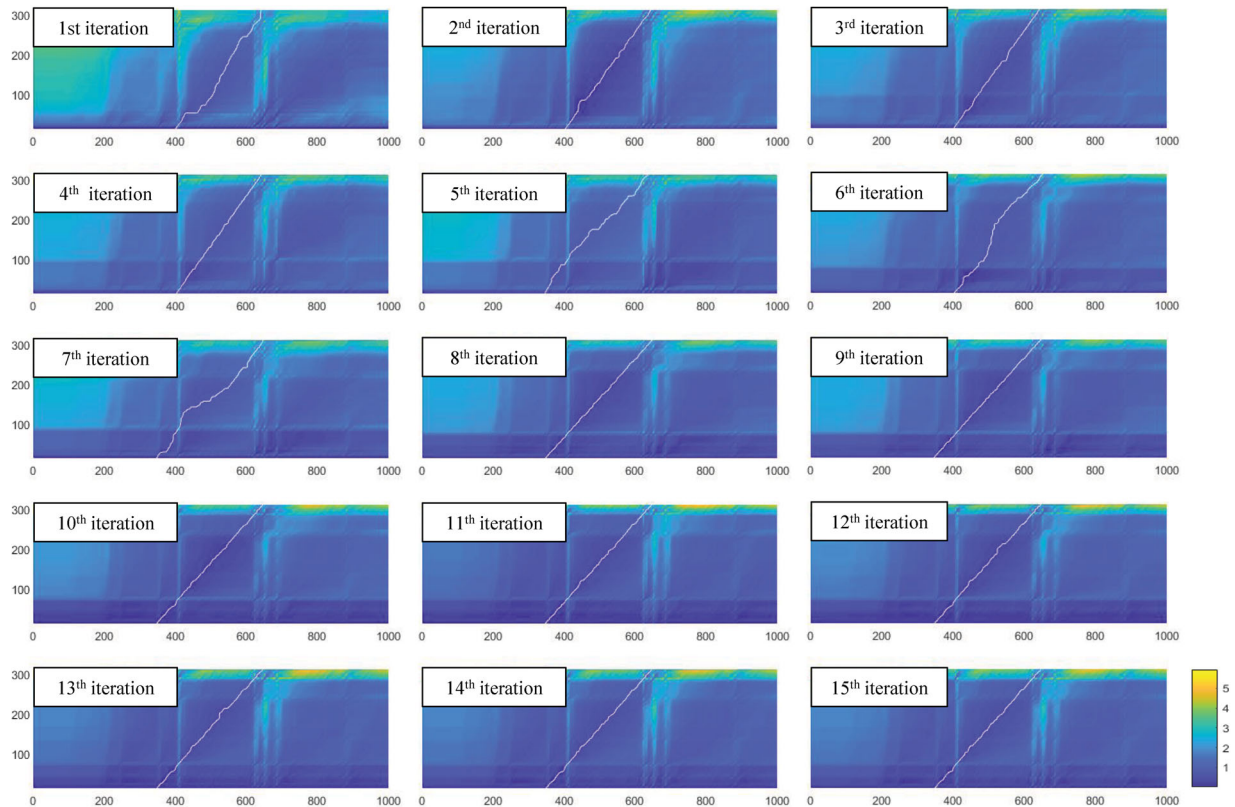
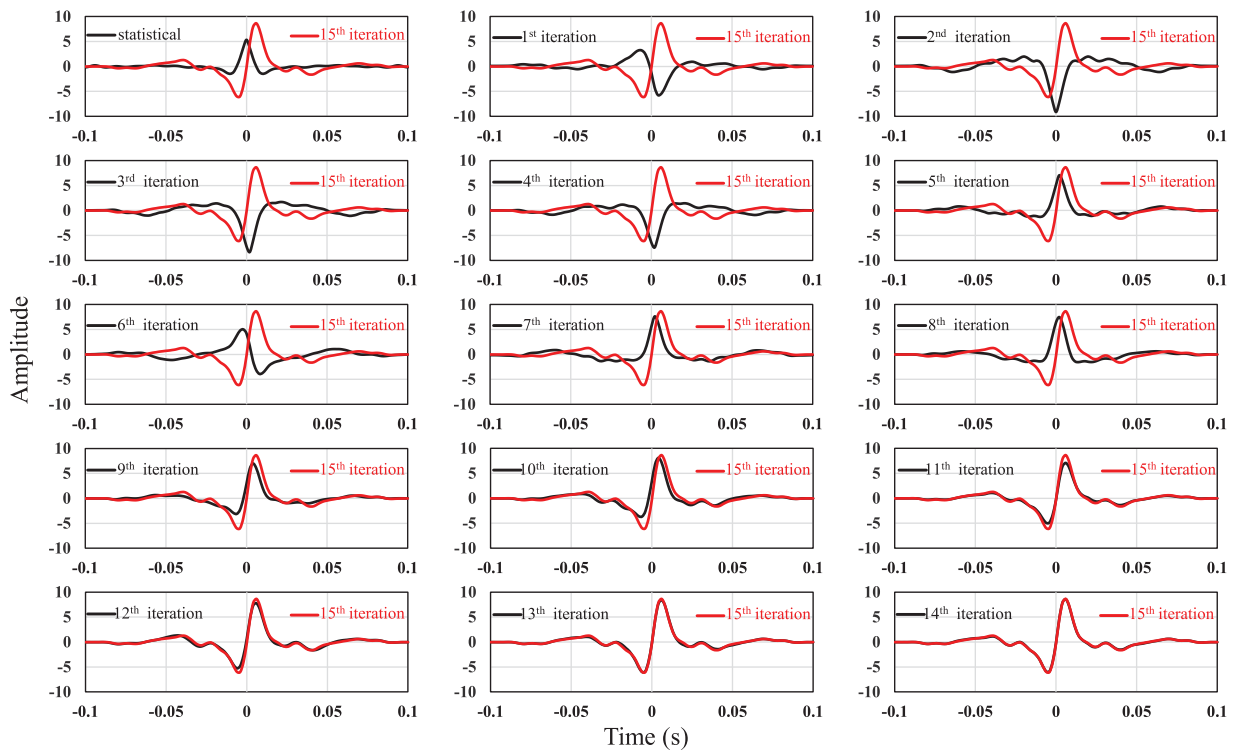


Figure 12. Accumulated error matrix overlaid with the optimum minimum cost path (white curve) in each iteration.

for each seismic-well tie. Figure 9 shows six representative results of automatic seismic-well ties in the first iteration for the  $0^\circ$ ,  $60^\circ$ ,  $120^\circ$ ,  $180^\circ$ ,  $240^\circ$  and  $300^\circ$  phase-rotated wavelets. We automatically performed 360 seismic-well ties for each iteration and need  $\sim 30$  s for each iteration. Figure 10 shows the cross-correlation

coefficient varying with the phases of the wavelets. We obtained the cross-correlation coefficients in Figure 10 by comparing the similarity between synthetic and seismic traces after the seismic-well ties. According to the cross-correlation coefficients shown in Figure 10, the best phase for the wavelet in the first iteration is  $125^\circ$ .





**Figure 13.** Wavelets with the best phases in each iteration. The black and red curves are the wavelet with the best phase and the final best wavelets, respectively.

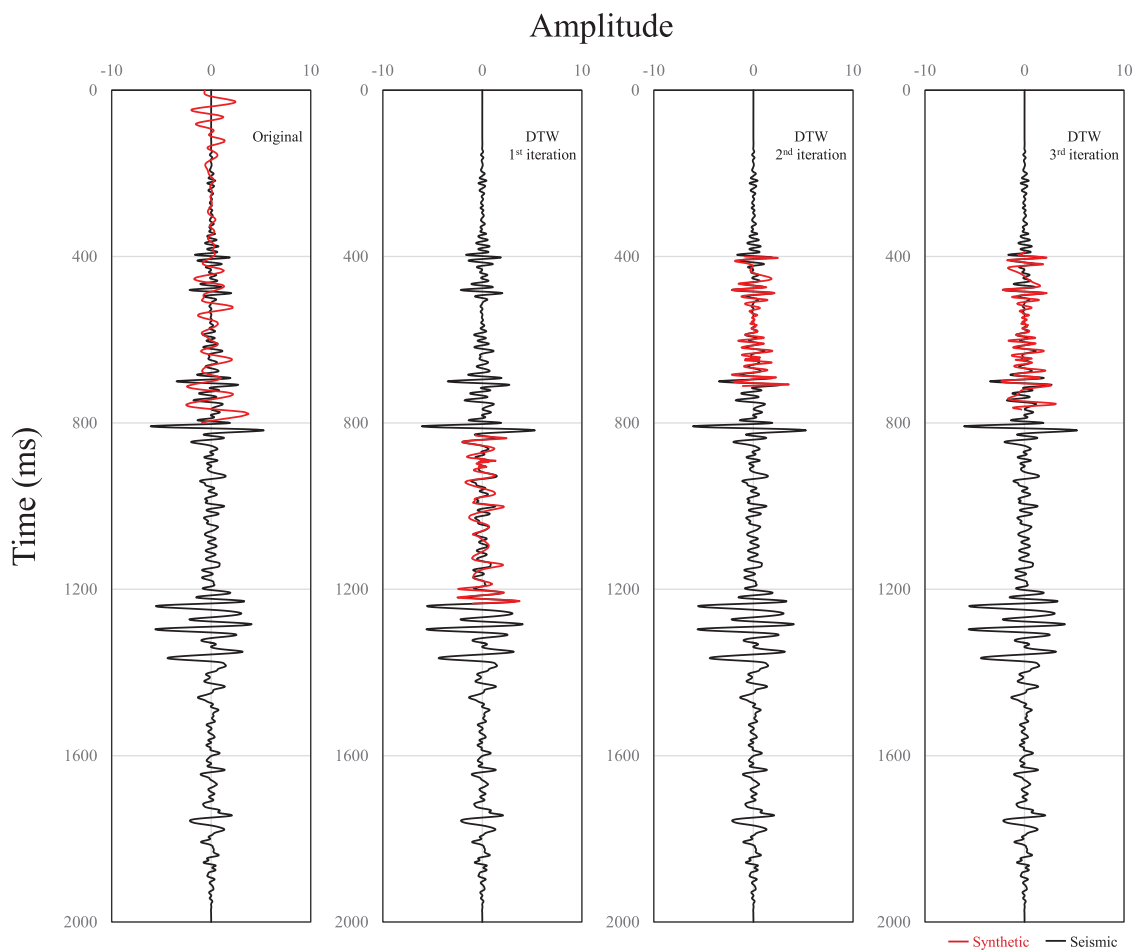


**Figure 14.** Test of dynamic time warping (DTW) using real data. The first panel shows the original synthetic seismogram (red) overlaid on the seismic trace (black), the second to fourth panels show the results of the first to third iterations for a seismic trace (black) and tied synthetic seismogram (red). The synthetic seismogram is tied to the wrong position and shows some abrupt changes in the time–depth relationship.

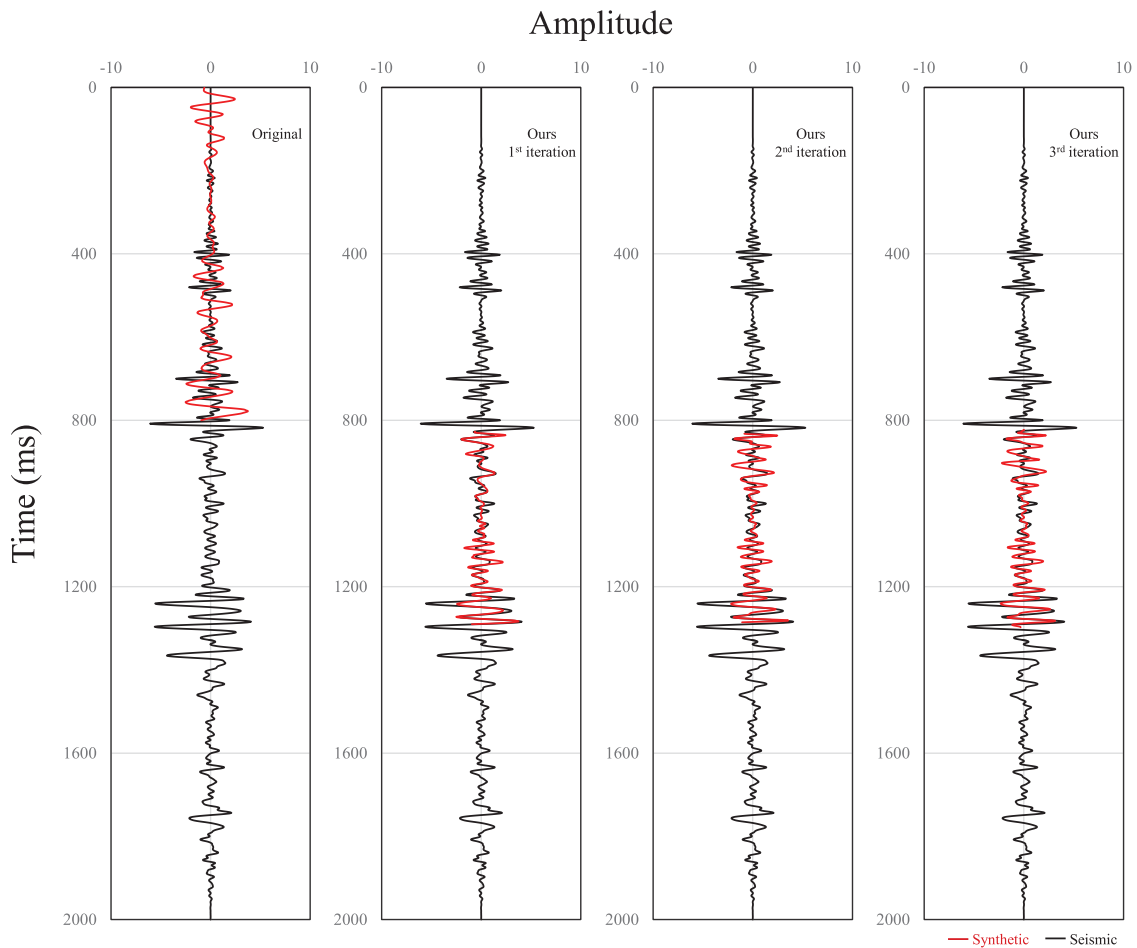


**Figure 15.** The proposed method applied to real seismic data. The first panel shows the original synthetic seismogram (red) overlaid on the seismic trace (black), the second to fourth panels show the results of the first to third iterations for a seismic trace (black) and tied synthetic seismogram (red). Noted that the tied synthetic seismogram meets the defined threshold and an excellent seismic-well tie is obtained after three iterations.

The final processing in each iteration is updating the time–depth relationship according to the seismic-well tie with the maximum correlation coefficient.

In our case, there are negligible changes for both wavelets and seismic-well ties after 15 iterations. Figure 11 shows the seismic-well tie for each iteration. The red and black curves are the synthetic and seismic traces, respectively. Note the change in the seismic-well tie is negligible from the eighth iteration. Figure 12 shows the accumulated error matrix and optimal warping minimum cost path (white curve). Figure 13 shows wavelets changing with the iteration number of the seismic-well tie. The black and red curves are the wavelet with best phase in each iteration and the final optimum wavelet, respectively. Note that there are negligible changes in the shape and phase of the seismic wavelet after the 15th iteration. We obtain our best wavelet after 15 iterations in our application according to the criteria defined in Equation (6).

### Comparison with conventional DTW

To illustrate the robustness of our proposed workflow, we also compare our method with conventional DTW.

We selected the same seismic and well log data from the Fort Worth Basin. We iteratively applied DTW and our method to align the synthetic seismogram from the well log with the real seismic trace. The black and red curves in the first panel of Figures 14 and 15 are the real seismic trace and original synthetic seismogram, respectively. The black and red curves in the second, third and fourth panels of Figures 14 and 15 are the first to third iterations of a real seismic trace and tied synthetic seismogram using DTW and our method, respectively. In Figure 14, the synthetic seismogram shows some abrupt velocity changes and, based on the well top data, the synthetic trace is tied to the wrong position in the seismic trace. Note that in Figure 15, our method gives greater cross-correlation, the synthetic trace has tied to the right position in seismic trace and the change in the time–depth relationship meets the defined threshold.

### Conclusions

We present a novel workflow to estimate the wavelet phase automatically. Here, we first improve the DTW algorithm by adding a second derivative weight to

the error matrix computation. The weighted term is designed to avoid severe stretching or squeezing of the synthetic trace during seismic-well ties. We then obtain the best phase of a wavelet by performing an iteratively automatic seismic-well tie using our proposed modified DTW algorithm. The application and comparison illustrate that our workflow not only obtains the best wavelet phase for the seismic-well tie, but also improves the quality of the seismic-well tie. Moreover, our workflow also expedites wavelet phase estimation and seismic well tying when compared with a manual seismic-well tie.

## Acknowledgements

The authors thank the CGG providing the academic license for HampsonRussell software. The authors used Hampson-Russell software to estimate the statistical wavelet in this research. The revised version of this paper benefitted tremendously from the comments and suggestions of Associate Editor, Dr Jianxiong Chen, reviewer Dr Xinming Wu, and other two anonymous reviewers.

## Disclosure statement

No potential conflict of interest was reported by the authors.

## References

- Buland, A., and H. Omre. 2003. Joint AVO inversion, wavelet estimation and noise-level estimation using a spatially coupled hierarchical Bayesian model. *Geophysical Prospecting* 51: 531–50.
- Edgar, J., and M. van der Baan. 2011. How reliable is statistical wavelet estimation? *Geophysics* 76 no. 4: V59–68.
- Hale, D. 2013. Dynamic warping of seismic images. *Geophysics* 78 no. 2: S105–15.
- Hampson, D. 2007. Theory of the Strata program: Technical report, CGG Hampson-Russell.
- Herrera, R.H., and M. van der Baan. 2012. Guided seismic-to-well tying based on dynamic time warping, SEG Expanded Abstracts.
- Herrera, R.H., S. Fomel, and M. van der Baan. 2014. Automatic approaches for seismic to well tying. *Interpretation* 2 no. 2: SD9–17.
- Levy, S., and D.W. Oldenburg. 1987. Automatic phase correction of common-midpoint stacked data. *Geophysics* 52: 51–9.
- Müller, M. 2007. *Dynamic time warping in information retrieval for music and motion*. Springer, Berlin.
- Muñoz, A., and D. Hale. 2012. Automatically tying well logs to seismic data, CWP-725.
- Muñoz, A., and D. Hale. 2015. Automatic simultaneous multiple well ties. *Geophysics* 80 no. 5: IM45–51.
- Nyman, D.C., M.J. Parry, and R.D. Knight. 1987. Seismic wavelet estimation using well control, SEG Expanded Abstracts, 211–13.
- Richard, V., and J. Brac. 1988. Wavelet analysis using well log information. SEG Expanded Abstracts, 946–9.
- Sakoe, H., and S. Chiba. 1978. Dynamic programming algorithm optimization for spoken word recognition. *IEEE Transactions on Acoustics, Speech, and Signal Processing* 26: 43–9.
- van der Baan, M. 2008. Time-varying wavelet estimation and deconvolution by kurtosis maximization. *Geophysics* 73 no. 2: V11–18.
- Walden, A.T., and R.E. White. 1984. On errors of fit and accuracy in matching synthetic seismograms and seismic traces. *Geophysical Prospecting* 32: 871–91.
- White, R.E. 1988. Maximum kurtosis phase correction. *Geophysical Journal International* 95: 371–89.
- White, R., and R. Simm. 2003. Tutorial: Good practice in well ties. *EAGE first break* 21: 75–83.
- Wiggins, R. 1978. Minimum entropy deconvolution. *Geoprospection* 16: 21–35.
- Wu, X., and G. Caumon. 2017. Simultaneous multiple well-seismic ties using flattened synthetic and real seismograms. *Geophysics* 82 no. 1: IM13–20.
- Yilmaz, Ö. 2001. *Seismic data analysis: processing, inversion, and interpretation of seismic data*. SEG, Tulsa.